# SPECTROSCOPIC MEASUREMENTS FOR POSSIBLE COMETARY DUST ANALOGUES*

Marcin Wesołowski †

University of Rzeszów, Faculty of Exact and Technical Sciences
Institute of Physics
Pigonia 1, 35-310 Rzeszów, Poland

Piotr Potera

University of Rzeszów, Faculty of Exact and Technical Sciences
Institute of Materials Science and Engineering
Pigonia 1, 35-310 Rzeszów, Poland

*Received 6 January 2026, accepted 30 March 2026, published online 2 July 2026*

We present new spectroscopic measurements for two dust analogue samples: walnut charcoal and willow charcoal. These measurements were performed in our laboratory using a Cary 5000 spectrometer equipped with an integrating sphere. This measurement setup enabled the measurement of hemispherical albedo as a function of wavelength in the range from 200 to 2500 nm. The obtained hemispherical albedo values ranged from 0.10 to 10.89%. Based on the obtained spectral profile measurements, the Bond albedo and geometric albedo values were calculated for selected possible analogues of refractory material present on cometary surfaces. The obtained mean Bond albedo value was 0.49%, while the mean geometric albedo value was 1.90%. These results were compared with macromolecular carbonaceous material present in cometary dust from comets. The obtained results were compared with measurements made by Rosetta/COSIMA, which showed that the cometary dust is dominated by macromolecular carbonaceous material, which is responsible for the very low albedo of comet 67P/Churyumov–Gerasimenko.

DOI:10.5506/APhysPolBSupp.19.3-A1

## 1. Introduction

The fundamental photometric parameter characterizing the optical properties of celestial bodies, including comets, is the albedo. It is defined as the ratio of reflected to incident solar radiation, typically integrated over a given

* Presented at the Planetary Science Conference, Kraków, Poland, 23–25 October, 2025.

† Corresponding author: mwesolowski@ur.edu.pl

wavelength range. In the case of comets, small Solar System bodies gravitationally bound to the Sun, it is customary to distinguish between geometric albedo and Bond albedo. The geometric albedo describes the reflectance of a surface observed at zero phase angle relative to that of an ideal Lambertian disk, whereas the Bond albedo accounts for the total fraction of incident radiation reflected in all directions and integrated over all wavelengths [1, 2].

For comets, the average geometric albedo is about 5%, meaning that only a small fraction of the incident solar radiation is reflected, while the majority is absorbed by the cometary nucleus. This absorbed energy contributes to heating the nucleus, driving the sublimation of volatile ices, as well as thermal re-emission and heat conduction into deeper layers. Such a low geometric albedo implies that cometary nuclei are among the darkest objects in the Solar System.

A well-studied example is comet 67P/Churyumov–Gerasimenko, investigated in detail during the Rosetta mission. Measurements performed by the OSIRIS (Optical, Spectroscopic and Infrared Remote Imaging System) and VIRTIS (Visible and Infrared Thermal Imaging Spectrometer) instruments showed that the geometric albedo is $6.5 \pm 0.2\%$ at a wavelength of $\lambda = 649$ nm [3]. It should be emphasized that this value is obtained within a finite instrumental bandpass rather than representing a strictly monochromatic quantity. In practice, it reflects the averaged response over the spectral sensitivity of the detector-filter system. Furthermore, the spectral range of the Rosetta instruments differs from that used in the present laboratory study. The OSIRIS system operated primarily in the visible range ($\sim$ 250–1000 nm), while VIRTIS extended into the near-infrared (up to $\sim$ 5000 nm), though under different viewing geometries and measurement conditions. In contrast, our laboratory measurements were performed over a continuous range from 200 to 2500 nm using an integrating sphere, providing hemispherical albedo under diffuse illumination. Therefore, a direct comparison between spacecraft-derived geometric albedo and laboratory hemispherical albedo requires caution, as differences arise from both spectral coverage and observational geometry. Nevertheless, the overlapping spectral region (especially within the visible range) allows for a meaningful qualitative comparison of the albedo of both cometary material and the investigated analogues.

Imaging of the nucleus revealed an almost uniformly dark surface, with only minor variations in surface brightness corresponding to locally higher albedo values. These variations are associated with localized sublimation activity and surface modification caused by numerous outbursts [4], which can expose subsurface layers [5]. One notable example is the Hapi region, where local brightness enhancements increased the geometric albedo to approximately 16% [3]. These observations demonstrate that albedo plays an important role in controlling the thermal balance and thus influencing cometary activity.

Obtaining pristine cometary material for laboratory studies is extremely challenging; therefore, various types of analog materials are increasingly used in experimental research [6–10]. Conducting laboratory studies, such as measurements of hemispherical albedo for dust analogues with controlled, well-characterized chemical composition is crucial for an accurate description of the cometary nucleus's sublimation activity. At the same time, it should be emphasized that even well-defined laboratory materials represent simplified systems compared to real cometary dust. Therefore, their compositional limitations must be taken into account when interpreting experimental results. In particular, they help to better constrain the energy balance governing sublimation processes, which in turn drive the morphological evolution of the cometary surface. As a result, the effective albedo may vary both spatially and temporally. From an instrumental perspective, it is important to distinguish between remote sensing measurements and laboratory spectroscopy. Spacecraft instruments typically measure bidirectional reflectance under specific illumination and phase angle conditions, whereas laboratory measurements with an integrating sphere provide hemispherical reflectance under nearly isotropic illumination. This difference is particularly relevant for dark, highly absorbing materials for which geometry-dependent effects may influence the derived albedo values.

The aim of this study is to perform new spectroscopic measurements of hemispherical albedo for selected dust analogs under terrestrial conditions. Based on the obtained spectral profiles, we estimate the Bond albedo of the studied materials under assumptions of solar spectral weighting and discuss the implications for their geometric albedo.

## 2. Sample preparation

For the spectroscopic measurements, we used two types of charcoal, which we produced ourselves. For this purpose, we selected two species of wood from our own resources: walnut wood (sample A) and willow wood (sample B). The wood was then crushed to facilitate the pyrolysis process, *i.e.*, the thermal treatment of wood. A ventilation block buried in the ground in the garden was used for this process. The wood was then placed in the block and ignited. After thoroughly burning, the process was interrupted by placing a thick sheet of metal on top of the block and sealing the escaping smoke with earth. This approach allowed the wood to degrade under high temperatures in anaerobic conditions. After the firing process ceased and cooled, the sheet of metal and the earth were carefully removed. The resulting charcoal was collected and placed in a container. For the other wood species, the entire procedure was repeated. The obtained charcoal was crushed and dry-sifted through standardized sieves. This way, for each

type of charcoal, we obtained four fractions with the following grain diameters: $0.06 < d_{gr} < 0.30$ mm; $0.30 < d_{gr} < 0.43$ mm; $0.43 < d_{gr} < 0.49$ mm, and $0.49 < d_{gr} < 1.50$ mm. Taking into account the two charcoal species and the respective fractions, the total number of tested samples was 8.

## 3. Spectroscopic measurement of hemispherical albedo

To conduct spectroscopic measurements, we used a Cary 5000 spectrometer equipped with an integrating sphere. This configuration allows for photometric measurement of hemispherical albedo in the range of 200 to 2500 nm. Measurement accuracy for wavelengths in the UV–VIS range is $\Delta\lambda = \pm 0.08$ nm, and for hemispherical albedo, $\Delta A_h = 0.07\%$ [11]. After startup, the spectrometer was calibrated using a reference spectrum to establish a baseline, which represents the signal level when the sample neither absorbs nor transmits light, but only reflects light according to the Labsphere-certified reflectance standard USRS-99-020 AS-01159-60. The zero line was calibrated against a quartz window.

We used the DRA (Diffuse Reflection Accessory) system to perform the measurements described in this paper. A detailed description of the entire measurement procedure was presented in our previous articles [10, 12]. Photometric measurements were performed for individual fractions and species of charcoal. The results of these measurements are presented in Figs. 1–2. Additionally, Figs. 3–4 show an example comparison of spectral profiles between two extreme fractions of the tested charcoal. It should be emphasized that each spectral profile contains over 2300 measurement points.

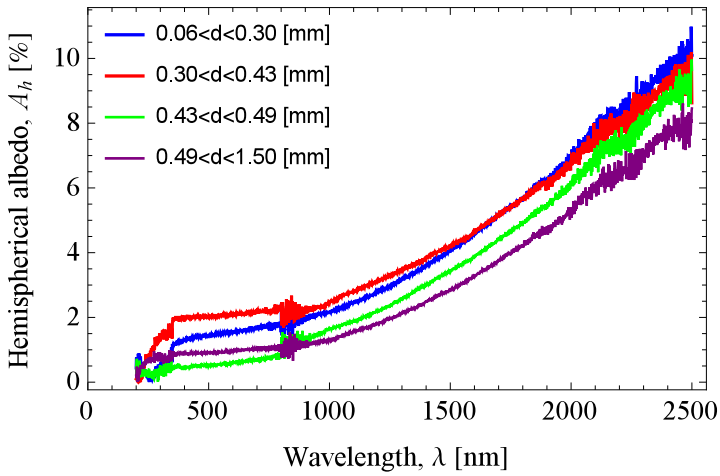


Fig. 1. Hemispherical albedo distribution as a function of wavelength from 200 to 2500 nm. The results presented refer to charcoal from walnut wood.

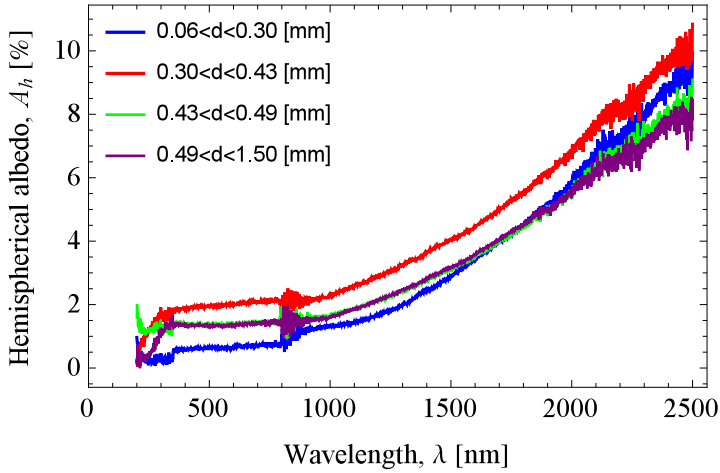


Fig. 2. Hemispherical albedo distribution as a function of wavelength from 200 to 2500 nm. The results presented refer to charcoal from willow wood.

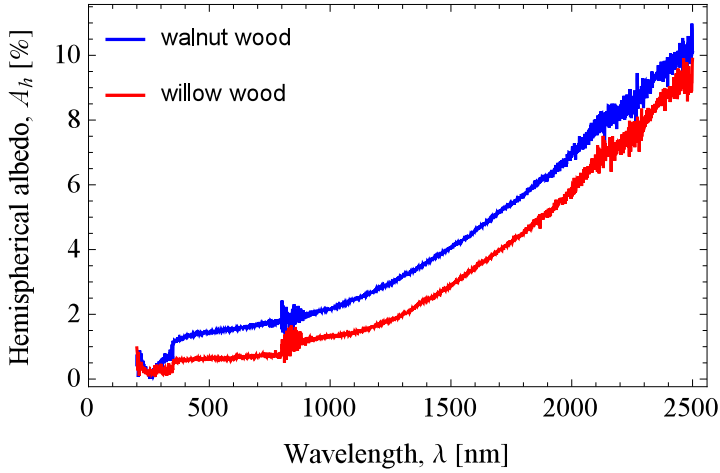


Fig. 3. Comparative analysis of the two extreme fractions of the tested charcoal for the fraction $0.06 < d_{\mathrm{gr}} < 0.30$ mm.

Based on the spectral profiles presented in Figs. 1–2, the following conclusions can be drawn:

1. The obtained hemispherical albedo values ranged from 0.10 to 10.89%. The main determinant of the hemispherical albedo value is the color of the sample. The darker the color, the lower the hemispherical albedo value.

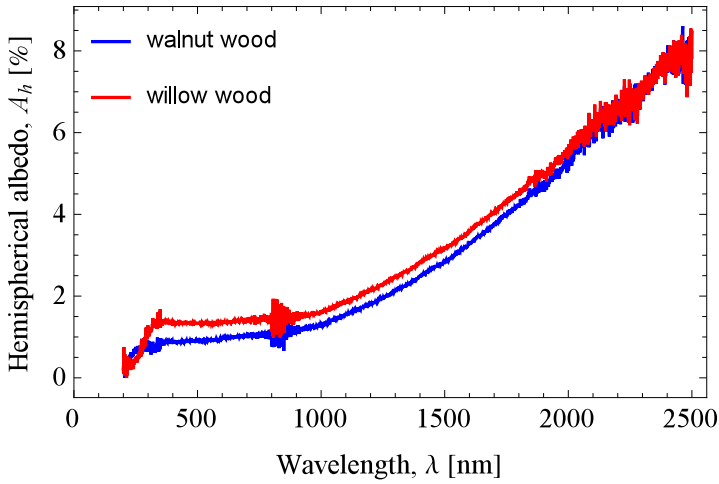


Fig. 4. Comparative analysis of the two extreme fractions of the tested charcoal for the fraction $0.49 < d_{\mathrm{gr}} < 1.50$ mm.

2. For all fractions, a monotonic increase in hemispherical albedo with wavelength can be observed. The increase is particularly pronounced in the near-infrared range, while in the UV–VIS range, hemispherical albedo values are low, indicating the dominance of absorption over scattering.

3. At around 900–1000 nm, a change in the slope of the curves is visible, which may be related both to the transition between the spectral ranges of the instrument and to the optical properties of the material being studied.

4. Across the entire spectral range, a systematic relationship between hemispherical albedo and grain diameter is observed: finer fractions are characterized by higher hemispherical albedo values compared to the coarsest fractions.

5. This effect is consistent with scattering theory, according to which a reduction in grain size leads to an increase in the number of phase boundaries and the effective scattering path, which increases the contribution of hemispherical albedo.

The above main conclusions were also confirmed in our previous research [10–13].

## 4. Geometric albedo

The basic photometric quantity commonly used in astronomy is the geometric albedo, defined as the ratio of the brightness of a body observed at zero phase angle to the brightness of a perfect Lambertian disk with the same radius and at the same distance. Using measurements of the hemispherical albedo, it is possible, under certain assumptions about the phase function, to estimate the geometric albedo. In the first step, one can calculate the bolometric albedo ($A_{\rm bol}$), which accounts for all the light scattered by a body across all wavelengths and all phase angles. This parameter can be calculated using the relationship

$$A_{\rm bol} = \frac{\int_{\lambda_1}^{\lambda_2} A_{\rm s}(\lambda) J_{\rm s}(\lambda, T_\odot) {\rm d}\lambda}{\int_{\lambda_1}^{\lambda_2} J_{\rm s}(\lambda, T_\odot) {\rm d}\lambda} \,. \tag{1}$$

In Eq. (1), the individual symbols mean: $A_{\rm s}(\lambda)$ is the spectral spherical albedo, $J_{\rm s}(\lambda, T_\odot)$ is approximately the Planck function for a black body at a temperature of 5770 K. The range of wavelengths in which the hemispherical albedo measurement was performed, *i.e.* from $\lambda_1 = 200$ nm to $\lambda_2 = 2500$ nm, was adopted as the integration limits. It should be noted that our experimental setup does not allow for direct measurement of the spherical albedo but the measured hemispherical albedo ($A_{\rm h}(\lambda)$) can be used as an upper limit for the spherical albedo [1]. In the second step, to determine the geometric albedo, the following two relations should be used:

$$A_{\rm B} \;=\; p_{\rm v} I = 2 p_{\rm v} \int_0^\pi \phi(\alpha) \sin\,\alpha \, {\rm d}\alpha \,, \tag{2}$$

$$A_{\rm B} \;=\; A_{\rm bol} I = 2 A_{\rm bol} \int_0^\pi \phi(\alpha) \sin\,\alpha \, {\rm d}\alpha \,. \tag{3}$$

In Eqs. (2)–(3), the individual symbols mean: $A_{\rm B}$ is the Bond albedo, $p_{\rm v}$ is the geometric albedo, $\phi(\alpha)$ is the ratio of apparent brightness at the phase angle $\alpha$ to the brightness at $\alpha = 0$, or in short, the phase function.

From Eqs. (2)–(3), it follows that:

$$p_{\rm v} \approx A_{\rm bol} \,. \tag{4}$$

Note that Eq. (4) is true for dark bodies, *i.e.*, with a low hemispherical albedo profile, which directly translates into the geometric albedo value. The value of the phase integral ($I$) in Eqs.(2)–(3) is equal to 0.253 [14].

Based on the results of spectroscopic measurements of hemispherical albedo (Figs. 1–2) and Eqs. (1)–(4), the Bond albedo and geometric albedo of the tested samples were calculated. The results of these calculations are presented in Table 1.

Table 1. The Bond albedo and geometric albedo values for charcoal coming from walnut wood (sample A) and willow wood (sample B). Let us emphasize that the obtained numerical values were influenced by the value of the phase integral, which, in turn, depends on the phase parameter.

| Sample | Grains diameter [mm] | Bond albedo [%] | Geometric albedo [%] |
|---|---|---|---|
| A | $0.06 < d_{gr} < 0.30$ | 0.54 | 2.15 |
| | $0.30 < d_{gr} < 0.43$ | 0.65 | 2.58 |
| | $0.43 < d_{gr} < 0.49$ | 0.35 | 1.39 |
| | $0.49 < d_{gr} < 1.50$ | 0.36 | 1.45 |
| B | $0.06 < d_{gr} < 0.30$ | 0.33 | 1.29 |
| | $0.30 < d_{gr} < 0.43$ | 0.63 | 2.49 |
| | $0.43 < d_{gr} < 0.49$ | 0.47 | 1.85 |
| | $0.49 < d_{gr} < 1.50$ | 0.46 | 1.82 |

Analyzing the obtained results, it can be noticed that:

1. The albedo of the studied analogs is very low, confirming their suitability as materials representing cometary dark matter.
2. A non-monotonic dependence of albedo on grain size is observed, with a clear maximum in the 0.30–0.43 mm range. For larger grain sizes, both the Bond and geometric albedo decrease, indicating increasing dominance of absorption processes.
3. The relationship between the Bond and geometric albedo remains consistent across all samples, confirming the validity of the adopted calculation procedure and suggesting a stable phase integral. The results emphasize the important role of surface granularity in controlling photometric properties.
4. Sample A exhibits higher albedo values than sample B only for the smallest grain sizes, whereas for larger grains, the opposite trend is observed. These differences are likely related to variations in surface morphology, internal structure, and porosity resulting from the distinct botanical origin of the samples.

5. The results demonstrate that both grain size and raw material type significantly influence the optical properties of charcoal, which should be taken into account when using such materials as laboratory analogues.
6. The obtained results provide valuable constraints for astrophysical and planetary applications, particularly in modeling radiative transfer and thermal balance of cometary surfaces.

## 5. Discussion

The paper presents an analysis of selected photometric parameters for two types of charcoal derived from walnut and willow wood. The measurements were performed using a Cary 5000 spectrometer equipped with an integrating sphere, enabling the determination of hemispherical albedo as a function of wavelength in the 200–2500 nm range. The obtained values depend on both the type of charcoal, reflecting its botanical origin, and the grain size distribution of the sample. The spectral profiles exhibit a generally increasing trend over most of the investigated wavelength range.

It should be emphasized that cometary dust is a complex and heterogeneous mixture composed of both carbonaceous material and mineral components, including silicates and sulfides. In contrast, charcoal, although carbon-rich, is not chemically pure carbon. Its composition depends on the precursor material and pyrolysis conditions, and typically includes residual inorganic components as well as oxygen- and hydrogen-bearing functional groups within the carbon structure. These impurities may influence the optical properties of charcoal, particularly in the ultraviolet and near-infrared regions, where additional absorption features may arise. Consequently, charcoal cannot be treated as a fully representative compositional analogue of cometary dust. However, it remains a useful first-order analogue due to its very low albedo and strongly absorbing nature, which are key characteristics of macromolecular carbonaceous material identified in cometary environments. Therefore, the present study should be interpreted as an investigation of simplified analogues that reproduce selected optical properties of cometary material rather than their full physicochemical complexity.

Spectroscopic measurements of dust analogues play an important role in constraining the thermal balance and sublimation processes of cometary nuclei. Sublimation-driven activity is responsible for the morphological evolution of the cometary surface. Due to the rapid and dynamic changes occurring on comet surfaces, especially after perihelion and during outbursts, the geometric albedo can vary significantly. This variability is associated with processes such as dust redistribution, exposure of subsurface layers, and changes in surface granularity. Consequently, accurate characterization of

albedo is essential for understanding and modeling the activity of cometary nucleus. Taking these limitations into account improves the robustness of the comparison and highlights the importance of combining laboratory measurements with *in situ* and remote sensing observations in order to better constrain the physical properties of cometary surfaces.

This work has been possible due to the support received from the Centre for Innovation and Transfer of Natural Sciences and Engineering Knowledge, University of Rzeszów, Poland.

## REFERENCES

[1] B. Hapke, «Theory of Reflectance and Emittance Spectroscopy»Topics in Remote Sensing, Vol. 3, *Cambridge University Press*, Cambridge, UK 1993.

[2] B. Hapke, *Icarus* **157**, 523 (2002).

[3] S. Fornasier *et al.*, *Astron. Astrophys.* **583**, A30 (2015).

[4] J.-B. Vincent *et al.*, *Mon. Not. R. Astron. Soc.* **462**, S184 (2016).

[5] M. Wesołowski, *Mon. Not. R. Astron. Soc.* **539**, 939 (2025).

[6] D. Haack *et al.*, *Astron. Astrophys.* **649**, A35 (2021).

[7] K.J. Kossacki, M. Wesołowski, G. Skóra, K. Staszkiewicz, *Icarus* **379**, 114946 (2022).

[8] A.D. Storrs, F.P. Fanale, R.S. Saunders, J.B. Stephens, *Icarus* **76**, 493 (1988).

[9] A. Rotundi *et al.*, *Science* **347**, aaa3905 (2015).

[10] M. Wesołowski, P. Potera, *Astron. Astrophys.* **686**, A248 (2024).

[11] M. Wesołowski, P. Potera, *Icarus* **416**, 116087 (2024).

[12] M. Wesołowski *et al.*, *Mon. Not. R. Astron. Soc.* **527**, 7613 (2023).

[13] M. Wesołowski, P. Potera, K. Kucab, *Planet. Space Sci.* **255**, 106027 (2025).

[14] M. Wesołowski *et al.*, paper under review, 2026.

[15] F. Preusker *et al.*, *Astron. Astrophys.* **583**, A33 (2015).